European Journal of Control (2011)1:19–29

DOI:10.3166/EJC.17.19–29

European Journal of Control

Optimal Control of Servo Actuators with Flexible Load and Coulombic Friction

Bahne Christiansen[1,**], Helmut Maurer[1,*], Oliver Zirn[2,***]

[1] Institut für Numerische Mathematik und Angewandte Mathematik, Westfälische Wilhelms-Universität Münster, Münster, Germany;
[2] Institut für Prozess- und Produktionsleittechnik, Technische Universität Clausthal, Clausthal-Zellerfeld, Germany

Feedback control and optimal control techniques are discussed for servo actuators that are widely used in micro-electro-mechanical systems (MEMS) technology of manufacturing. A typical servo actuator is the voice-coil motor used for actuating micro machine tool axes, bonding machines and hydraulic/pneumatic valve drives. State-of-the-art feedback control techniques are deficient with regard to high precision positioning and process duration. To improve on this deficiency, optimal control techniques are applied to a dynamical model of servo drives. Since Coulombic friction is modeled as sign function depending on the sign of the velocity, the optimal control problem belongs to the class of nonsmooth optimization problems. Time-optimal controls are computed for a variety of control bounds. It is shown that time-optimal controls are of bang-bang type and reduce transfer times considerably. Switching times are optimized directly by appropriate nonlinear programming methods. Optimal controls are studied under state constraints that limit deviations in positions and velocities of the slider and load mass. The goal of reducing such deviations can also be achieved by energy-optimal controls with larger transfer times. Real-time implementations of the computed optimal control signals indicate an excellent agreement between predicted trajectories and experimental results.

Keywords: Mechatronics, servo actuator, optimal control, switched systems, state constraints

1. Introduction

The drives in MEMS manufacturing machines are mostly based on linear electric motors. The linear motor shown in Figs. 1 and 2 is applied for servo axes in wire bonding machines, wafer steppers and ultra high precision positioning stages for laser cutters in MEMS manufacturing. Since this type of actuator is also very common for loudspeakers, it is called voice-coil motor. In the field of loudspeaker techniques, its function is the high-frequency conversion of electrical pulses into mechanical vibrations of the cone which produce the acoustic sound waves. State-of-the-art feedback control is deficient with regard to high precision positioning, vibration performance, as well as process duration. The goal of this paper is to improve on these deficiencies by applying optimal control methods.

In section 2, we introduce the linear dynamical model developed in [21]. However, due to Coulombic friction, state-dependent discontinuities may occur in the dynamics. Using state-of-the-art feedback control, the performance of the servo actuator is briefly discussed in section 3. To improve on some deficiencies of feedback control, nonsmooth optimal control problems are formulated in section 4. To compute optimal control and state

*Correspondence to: H. Maurer, E-mail: maurer@math.uni-muenster.de
**E-mail: bahnechr@math.uni-muenster.de
***E-mail: zirn@ipp.tu-clausthal.de

Received 7 September 2009; Accepted 10 May 2010
Recommended by M. do Rosario de Pinho, F.A.C.C. Fontes, D.F.M. Torres, A.J. van der Schaft

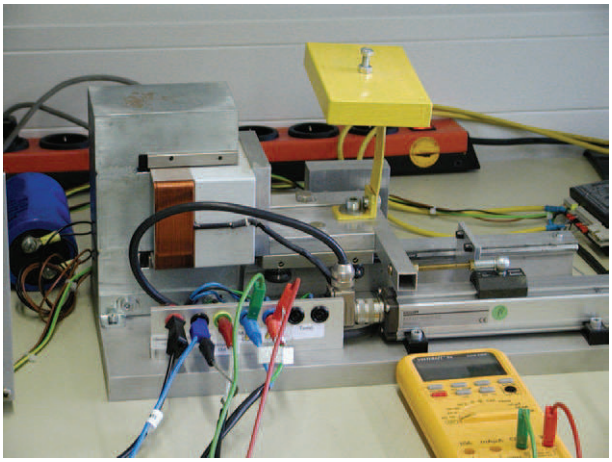

Fig. 1. Servo actuator (voice-coil motor) with real-time-system-control and flexible load. Test bench in the IPP mechatronics laboratory, Clausthal University of Technology.

trajectories, we discretize the control problem and apply large-scale nonlinear programming methods.

We determine both time-optimal and energy-optimal controls. In section 5, it is shown that time-optimal controls are of bang-bang type, where the number of degrees of freedom (switching times and final time) matches the number of terminal conditions. Changes in the sign of the slider velocity and thus discontinuities in the dynamics occur in a certain range of control bounds. Necessary and sufficient conditions are discussed on the basis of optimal multiprocess control problems [7, 8, 2]. Section 5.2 presents results on sensitivity derivatives of switching times under parameter variations. The excellent agreement between computed (predicted) optimal trajectories and experimental results is demonstrated in section 5.3. Some results for state-constrained optimal solutions are given in section 5.4. Finally, energy-optimal control solutions are briefly discussed in section 6. The paper is a modified and enlarged version of a paper presented at the IEEE CDC Conference 2008 [6]. Here, we give a more detailed analysis of time-optimal solutions and treat both state-constrained and energy-optimal solutions.

2. Dynamic Control Model of the Servo Actuator

Though the servo drive system (voice-coil motor) shown in Figs. 1 and 2 is a rather simple drive system, it incorporates all main characteristics of servo drives with feedback controlled motors in combination with flexible transmission devices and machine structure. The stator of the voice-coil motor is an iron core with rare earth permanent magnetic excitation. A copper coil is guided in the air gap on a slider. The coil and slider mass is denoted by m_1. The linear guide produces the Coulombic friction force F_R, which acts in

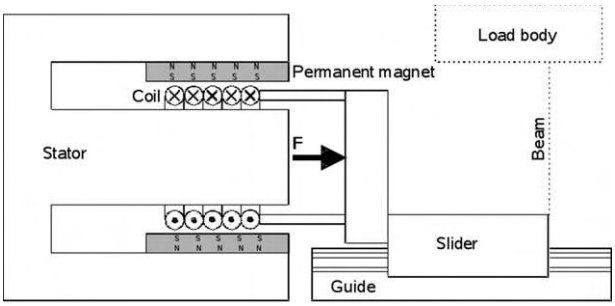

Fig. 2. Physical model of the servo actuator

Table 1. Physical parameters

DSPACE sampling time	$Ts = 0.1$ ms
Amplifier switching frequency	$f_{\mathrm{PWM}} = 50$ kHz
Amplifier intermediate voltage	$U_{\max} \le 10$ V
Coil resistance	$R = 2\,\Omega$
Coil inductivity	$L = 2$ mH
Force constant	$K_F = 12\,\mathrm{N/A}$
Back–EMF constant	$K_S = 12\,\mathrm{V\,s/m}$
Motor mass (slider, guide, coil)	$m_1 = 1.03$ kg
Load mass	$m_2 = 0.56$ kg
Spring constant	$K = 2.4\,\mathrm{kN/m}$
Guide friction force	$F_R = 2.1$ N
Linear encoder resolution	$\Delta x = 1\,\mu$m

the direction opposite to the slider velocity. A load mass m_2 is mounted on the slider with a spring k that has negligible damping. A coil current I induces the actuating force F (so called Lorenz force) given by the equation $F = K_F \cdot I$. The moving coil with the velocity v_1 generates a voltage U (also called back-EMF) according to $U = K_S \cdot v_1$. The system parameters are given in Table 1.

The dynamic process of the voice-coil motor is studied in the time interval $t \in [0, t_f]$ with t measured in seconds; the final time $t_f > 0$ is either fixed or free. The state variables are as follows: The motor mass position $x_1(t)$, the motor mass velocity $v_1(t)$, the load mass position $x_2(t)$, the load mass velocity $v_2(t)$ and the electric current $I(t)$. The input variable (control) of the motor is the voltage $U(t)$. The dynamic equations are given by the following linear differential system, where as usual, the dot denotes the time derivative:

$$\dot{x}_1 = v_1, \tag{1}$$

$$\dot{v}_1 = \frac{1}{m_1}\,[\,K_F \cdot I - K \cdot (x_1 - x_2) - F_R \cdot sign(v_1)\,], \tag{2}$$

$$\dot{x}_2 = v_2, \tag{3}$$

$$\dot{v}_2 = \frac{K}{m_2} \cdot (x_1 - x_2), \tag{4}$$

$$\dot{I} = \frac{1}{L}\,[\,U - R \cdot I - K_S \cdot v_1\,]. \tag{5}$$

The Coulombic friction force is modeled by the expression $-F_R \cdot sign(v_1)$ in equation (2), where the sign function is defined by

$$sign(v_1) = \left\{ \begin{array}{ll} 1, & \text{if } v_1 > 0 \\ 0, & \text{if } v_1 = 0 \\ -1, & \text{if } v_1 < 0 \end{array} \right\}.$$

For the monorail guides applied here, stick-slip and viscous friction can be neglected due to the small operation velocities and the very small difference between Coulombic friction and stiction. The Coulombic friction force $-F_R \cdot sign(v_1)$ induces a state-dependent jump in (2) and thus leads to an ordinary differential equation (ODE) with a non-differentiable right hand side. Therefore, the optimal control problem formulated in section 4 falls into the class of *nonsmooth* optimization problems.

The ODE (2) is slightly inexact and simplifies the real behaviour of the motor, since it does not reflect accurately the static friction in a position of rest. To actuate the slider from a position of rest, the absolute value of the accelerating force

$$F_a = K_F \cdot I - K \cdot (x_1 - x_2)$$

has to exceed the static Coulombic friction force F_R. This deficiency can be removed by adding the term

$$\min \left\{ -F_a, -F_R \cdot \frac{F_a}{|F_a|} \right\} \quad (\text{when} \quad v_1 = 0) \qquad (6)$$

in the bracket on the right hand side of equation (2). In the numerical calculations we replace the condition $v_1 = 0$ in (6) by $|v_1| \leq \epsilon_v$ with an appropriate small constant $\epsilon_v > 0$. To simplify the analysis, we ignore this term in the following.

The control constraint is given by

$$-U_{\max} \leq U(t) \leq U_{\max}, \quad 0 \leq t \leq t_f, \qquad (7)$$

where $U_{\max} \leq 10\,V$ for mechanical reasons. For the state vector $x = (x_1, v_1, x_2, v_2, I)^* \in \boldsymbol{R}^5$, the initial and terminal boundary conditions are chosen as

$$x(0) = (0,0,0,0,0)^*, \quad x(t_f) = (0.01, 0, 0.01, 0, 0)^*, \qquad (8)$$

where positions are measured in meters.

3. Feedback Control Performance

In typical industrial applications, the voice-coil motor servo axis is equipped with a numerical control system for setpoint generation and a cascade feedback controller as is shown in Fig. 3. Fig. 4 shows the measured and simulated performance of the motor/slider as well as the load mass for ramp and step response. This elucidates the fact that the system requires very soft setpoint values (i.e., a setpoint ramp with small slope) to avoid overshoot and vibrations for the load. The application of state space feedback control or H_∞-control in combination with feedforward filters can increase damping but yields no significant positioning performance enhancement. Thus realistic state-of-the-art control techniques enable this voice-coil motor axis to reach positioning times of 0.3 to 0.4 s for 10 mm positioning task given in (8).

4. Optimal Control Model of a Servo-Actuator

The system (1)–(5) can be written as

$$\dot{x} = f(x, U) = Ax + BU + C \cdot sign(v_1) \qquad (9)$$

with a 5×5-matrix A and vectors B, $C \in \boldsymbol{R}^5$ defined by

$$A = \begin{pmatrix} 0 & 1 & 0 & 0 & 0 \\ -\dfrac{K}{m_1} & 0 & \dfrac{K}{m_1} & 0 & \dfrac{K_F}{m_1} \\ 0 & 0 & 0 & 1 & 0 \\ \dfrac{K}{m_2} & 0 & -\dfrac{K}{m_2} & 0 & 0 \\ 0 & -\dfrac{K_S}{L} & 0 & 0 & -\dfrac{R}{L} \end{pmatrix},$$

$$B = \begin{pmatrix} 0 \\ 0 \\ 0 \\ 0 \\ \dfrac{1}{L} \end{pmatrix}, \quad C = \begin{pmatrix} 0 \\ -F_R \\ 0 \\ 0 \\ 0 \end{pmatrix}.$$

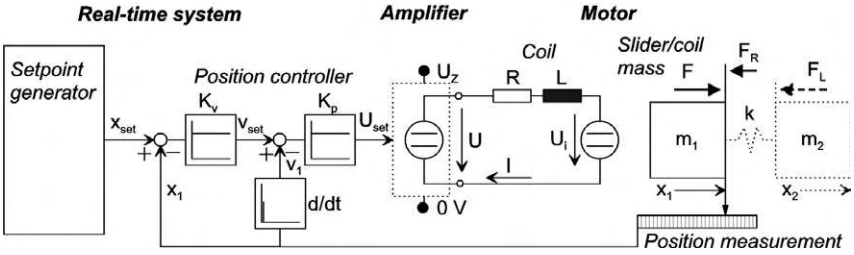

Fig. 3. Feedback control of the servo actuator

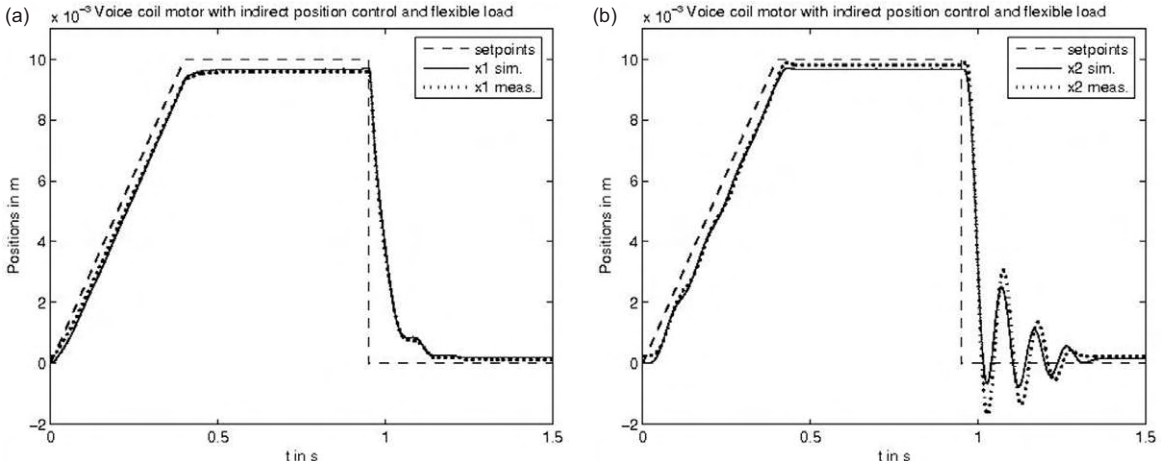

Fig. 4. Ramp and step response measured (a) at the slider and (b) at the load mass.

We consider two types of cost functionals to be minimized subject to the conditions (1)–(8): either the time-optimal case,

$$\text{minimize the final time} \quad t_f, \tag{10}$$

or a criterion with a quadratic penalty on the control variable that will be referred to as the "energy optimal" case,

$$\text{minimize} \quad \int_0^{t_f} U(t)^2 dt \quad \text{for fixed} \;\; t_f > 0. \tag{11}$$

Of course, the fixed final time t_f in (11) must be larger than the minimal time in (10). To avoid larger oscillations in the servo actuator system, state constraints of the form

$$-c_v \le v_1(t) - v_2(t) \le c_v, \tag{12}$$

$$-c_x \le x_1(t) - x_2(t) \le c_x, \tag{13}$$

are imposed with prescribed constants $c_v > 0$, $c_x > 0$. Due to space limitations, only the state constraint (12) for the velocities will be addressed in section 5.4. The state constraint (13) is difficult to handle numerically since it is of third order; cf. the definition of the order of a state constraint in [11, 15]. This may lead to chattering junctions of bang-bang and boundary arcs as it has actually been observed in computations. For large final times t_f, energy-optimal solutions are shown to satisfy the state constraints (12) and (13) with bounds of practical relevance; cf. the brief exposition in section 6.

5. Time-Optimal Control

5.1. Computation of Bang-Bang Controls

Computations in the time-optimal case show that the optimal solution is a concatenation of finitely many bang-bang arcs with at most one subarc $[t_1^v, t_2^v]$ with negative velocity $v_1(t) < 0$ for $t_1^v < t < t_2^v$. Let us support these findings by theoretical considerations. The optimal solution is a combination of arcs $[t_{k-1}, t_k]$ where either $v_1(t) > 0$ or $v_1(t) < 0$ or $v_1(t) = 0$ holds. Since the entire solution is time-optimal, the control on each subarc which transfers the intitial point $x(t_{k-1})$ to the final point $x(t_k)$ must be time-optimal.

The linear system (9) is completely controllable, since the 5×5 Kalman matrix $D = (B, AB, A^2B, A^3B, A^4B)$ has maximal rank 5. Hence, the time-optimal control is bang-bang with $U(t) = \pm U_{\max}$; cf. [12]. This property allows us to exclude subarcs with $v_1(t) = 0$. Intuitively one would argue that such subarcs are not compatible with time-optimality. The proof proceeds by contradiction. If $v_1(t) = 0$ holds, then equation (1) implies that $x_1(t) = x_{1c}$ is a constant and thus equation (2) yields $K_F \cdot I - K(x_{1c} - x_2) = 0$ in view of $F_R\, sign(v_1) = 0$. By differentiating the last equality using (5) we obtain

$$K_F\,(\pm U_{\max} - R \cdot I) + K v_2 = 0.$$

Differentiating this relation using equations (5) and (4) and the above equality $K(x_{1c} - x_2) = 0 = K_F \cdot I$ we arrive at the relation

$$0 = K_F R\,(\pm U_{\max} - R \cdot I)/L^2 + I K_F K/m_2.$$

Hence, $I(t)$ must be a constant which implies $\dot{I} = \pm U_{\max} - R \cdot I = 0$ in view of (5). Inserting this into the preceding equality we get $I = 0$ which gives a contradiction to $\pm U_{\max} - R \cdot I = 0$ and $U_{\max} > 0$. This completes the proof that there is no subarc with $v_1(t) = 0$.

Thus we may view the optimal control problem as a *multiprocess optimal control problem* where the dynamics (2) becomes discontinuous when $v_1(t)$ changes sign. We can apply the necessary optimality conditions for *multiprocess optimal control problem* in Clarke, Vinter [7, 8]

and Augustin, Maurer [2]. The Hamiltonian function is defined by

$$H(x, \lambda, U) = 1 + \lambda\,(Ax + BU + C\,\mathrm{sign}\,(v_1)),$$

where $\lambda = (\lambda_{x_1}, \lambda_{v_1}, \lambda_{x_2}, \lambda_{v_2}, \lambda_I) \in \boldsymbol{R}^5$ is the adjoint variable. The adjoint equations $\dot{\lambda} = -H_x = -\lambda A$ are given by the linear equation

$$\begin{aligned}
\dot{\lambda}_{x_1} &= \frac{K}{m_1}\,\lambda_{v_1} - \frac{K}{m_2}\,\lambda_{v_2}, \qquad \dot{\lambda}_{v_1} = -\lambda_{x_1} + \frac{K_S}{L}\,\lambda_I, \\
\dot{\lambda}_{x_2} &= -\frac{K}{m_1}\,\lambda_{v_1} + \frac{K}{m_2}\,\lambda_{v_2}, \quad \dot{\lambda}_{v_2} = -\lambda_{x_2}, \qquad (14) \\
\dot{\lambda}_I &= -\frac{K_F}{m_1}\,\lambda_{v_1} + \frac{R}{L}\,\lambda_I.
\end{aligned}$$

Note that the adjoint equations do not depend on the friction constant F_R, since the term $C \cdot sign(v_1)$ in (9) is piecewisely constant. Boundary conditions are not prescribed for $\lambda \in \boldsymbol{R}^5$, since the initial and terminal conditions are specified for each of the five state variables in (8). The control that minimizes the Hamiltonian is determined by

$$U(t) = -\mathrm{sign}\,(\lambda_I(t))\,U_{\max}\,. \qquad (15)$$

To solve the optimal control problem, we discretize the problem using Euler's method or Heun's second order integration method. The resulting large-scale optimization problem is implemented using the modeling language AMPL (Fourer et al. [9, 10]) and is solved by the nonlinear programming code IPOPT (Wächter, Biegler [20]). Using $N = 20000$ grid points, our computations show that, for all values of $U_{\max} > 0$ the control has the following structure with 4 switching times $0 < t_1 < t_2 < t_3 < t_4 < t_f$ and the free final time $t_5 := t_f$:

$$U(t) = \left\{ \begin{array}{rl} U_{\max} & \text{for } 0 \le t < t_1 \\ -U_{\max} & \text{for } t_1 < t < t_2 \\ U_{\max} & \text{for } t_2 < t < t_3 \\ -U_{\max} & \text{for } t_3 < t < t_4 \\ U_{\max} & \text{for } t_4 < t \le t_5 \end{array} \right\}. \qquad (16)$$

This control structure is not surprising, since one intuitively expects that five degrees of freedom, namely the five variables t_1, t_2, t_3, t_4, t_f, suffice to satisfy the five terminal conditions in (8). This discretization and optimization approach provides switching times that are correct up to 3-4 decimals. After determining the correct control structure, we apply a refined numerical method for computing the switching times with high precision. Due to the control structure (16), the bang-bang control problem is equivalent to an optimization problem, where the switching times t_i $(i = 1, 2, 3, 4)$ and the free final time t_f are considered as the only optimization variables; cf. Agrachev *et al.* [1], Osmolovskii, Maurer [19]. Instead of optimizing the switching times directly, we use the arc-parametrization method in Maurer *et al.* [16] to optimize the *arclengths* of the bang-bang arcs defined by

$$\xi_j = t_j - t_{j-1},\ (j = 1, 2, 3, 4, 5), \quad t_0 := 0, \quad t_5 := t_f.$$

This method can be implemented using the Fortran code NUDOCCCS developed by Büskens [3].

The sign distribution of the motor mass velocity $v_1(t)$ in $[0, t_f]$ depends crucially on the value $U_{\max}$ of the control bound. We can summarize our numerical results as follows. There exist two control bounds

$$U^1_{\max} := 1.85476, \quad U^2_{\max} = 2.38327,$$

with the following property: for all bounds $U_{\max}$ with

$$U^1_{\max} < U_{\max} < U^2_{\max} \qquad (17)$$

we have $v_1(t) > 0$ for all $0 < t < t_f$, while for

$$U_{\max} < U^1_{\max} \quad \text{or} \quad U^2_{\max} < U_{\max} \qquad (18)$$

the velocity $v_1(t)$ has the sign distribution

$$v_1(t) = \left\{ \begin{array}{ll} > 0 & \text{for } 0 < t < t^v_1 \\ < 0 & \text{for } t^v_1 < t < t^v_2 \\ > 0 & \text{for } t^v_2 < t < t_f \end{array} \right\}. \qquad (19)$$

The intermediate times t^v_1, t^v_2 satisfy

$$t_1 < t^v_1 < t_2 < t^v_2 < t_3.$$

For bounds $U_{\max}$ satisfying the inequalities in (18) we thus encounter a *multiprocess* control problem with two different dynamical systems defined either by the friction force F_R or $-F_R$ in equation (2). The velocity $v_1(t)$ is zero at the points t^v_1 and t^v_2, which yields two additional interior conditions

$$v_1(t^v_1) = 0, \quad v_1(t^v_2) = 0. \qquad (20)$$

Applying the necessary conditions in [8], [2], we find that the adjoint variable λ_{v_1} may have jumps according to

$$\lambda_{v_1}((t^v_k)+) = \lambda_{v_1}((t^v_k)-) + \rho_k, \qquad k = 1, 2, \quad (21)$$

where ρ_k, $k = 1, 2$, are multipliers obtained from the transversality conditions [2], eq. (32)–(34). Computations show that $\rho_k = 0$, $k = 1, 2,$; hence, the adjoint variable $\lambda_{v_1}(t)$ is *continuous* at t^v_k, $k = 1, 2$.

We choose the control bounds $\mathbf{U}_{\max} = \mathbf{2}$ and $\mathbf{U}_{\max} = \mathbf{3}$ to illustrate the different control strategies described in (17) and (18).

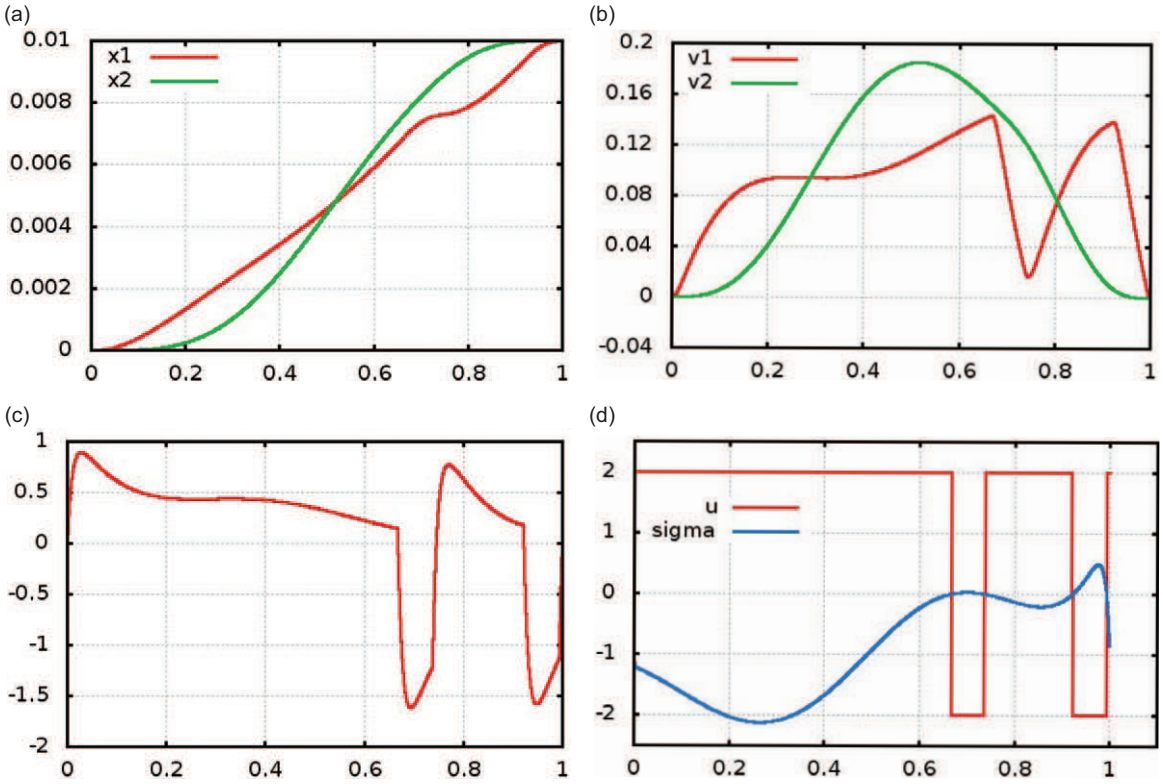

Fig. 5. $\mathbf{U_{max} = 2}$: time-optimal solution on normalized time interval [0, 1]; (a) positions $x_1(t), x_2(t)$; (b) velocities $v_1(t), v_2(t)$; (c) electric current $I(t)$; (d) control $U(t)$ and scaled switching function $\sigma(t)$ satisfying (15); enlarged time axis to better display the tiny terminal bang-bang arc.

Case $\mathbf{U_{max} = 2}$. Fig. 5 displays the optimal state and control variables for the control constraint $U_{\max} = 2$. Recall from (17) that $v_1(t)$ remains positive for $0 < t < t_f$. The switching times and final time are computed as

$$t_1 = 0.074140, \quad t_2 = 0.0820268, \quad t_3 = 0.101444,$$
$$t_4 = 0.110420, \quad \mathbf{t_f = 0.111184}.$$

The initial value of the adjoint variable $\lambda(t) \in \boldsymbol{R}^5$ satisfying the adjoint equation (14) is given by

$$\lambda(0) = (-4.82918, -0.100808, -4.09481, \\ -0.057766, -0.001074).$$

With these values, the reader may verify that the switching function

$$\sigma(t) := H_U(t) = \lambda_I(t)/L \tag{22}$$

obeys the control law (15) with high accuracy; Fig. 5(d). The local optimality of this trajectory follows from the fact that the 5×5 Jacobian matrix of the terminal conditions computed with respect to the switching times and final time is a regular matrix. Hence, first order sufficient conditions are satisfied for this time-optimal control problem; cf. [17, 19].

Case $\mathbf{U_{max} = 3}$. The optimal state and control variables are depicted in Fig. 6. In view of (18) and (19), we have $v_1(t) < 0$ for $t_1^v < t < t_2^v$. Here, the times t_1^v, t_2^v are treated as additional optimization variables which allows us to apply again the arc-parametrization method in [16]. We obtain the switching times, the two intermediate times and the final time

$$t_1 = 0.0416854, \quad t_1^v = 0.0480052, \quad t_2 = 0.0525894,$$
$$t_2^v = 0.0563559, \quad t_3 = 0.0786491, \quad t_4 = 0.0878590,$$
$$\mathbf{t_f = 0.0886180}.$$

The computed initial value of the adjoint variable is

$$\lambda(0) = (-4.40300, -0.065128, 1.34424, \\ -0.005169, -0.00692).$$

Again, the switching function $\sigma(t) := \lambda_I(t)/L$ satisfies the control law (15) precisely; cf. Fig. 6(d).

5.2. Sensitivity Analysis of Arclengths

We give a brief outlook on sensitivity analysis of optimal solutions when system parameters are subject to perturbations. For purpose of demonstration, we choose the

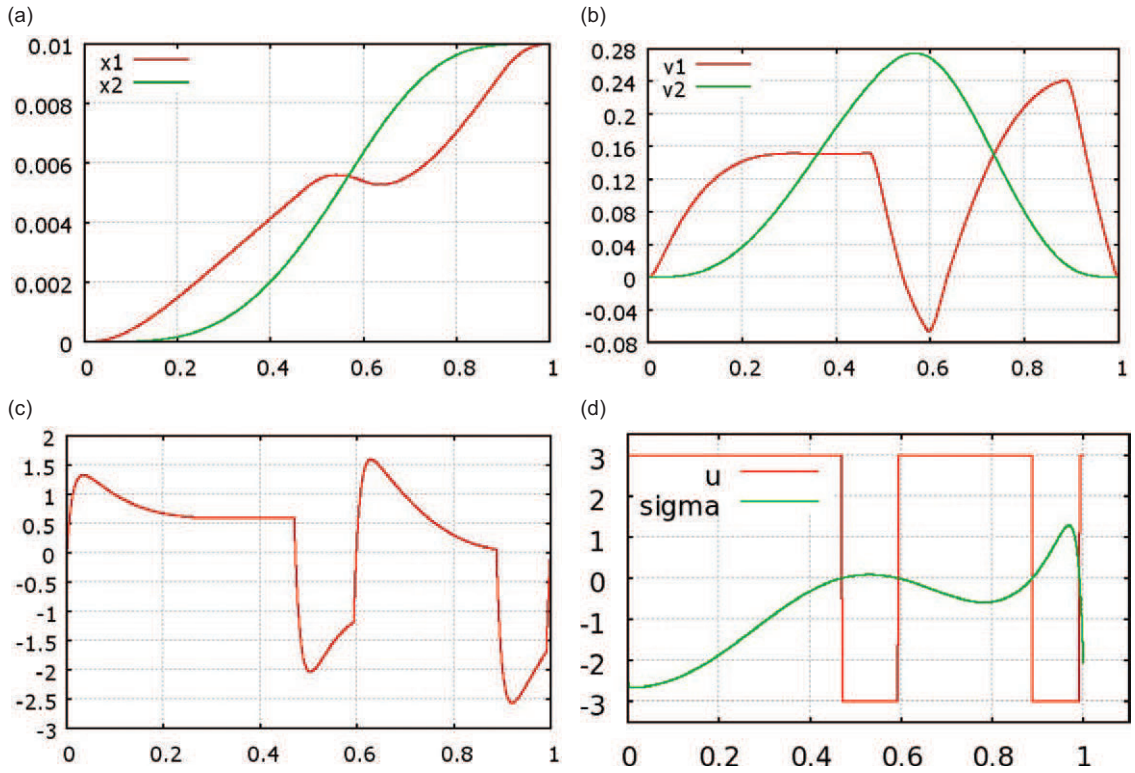

Fig. 6. $\mathbf{U_{max}} = \mathbf{3}$: time-optimal solution on normalized time interval $[0, 1]$; (a) positions $x_1(t), x_2(t)$; (b) velocities $v_1(t), v_2(t)$; (c) electric current $I(t)$; (d) control $U(t)$ and scaled switching function $\sigma(t)$ satisfying (15).

bound $\mathbf{U_{max}} = \mathbf{3}$. The corresponding optimal control has 7 subarcs with arclengths

$$\xi_1 = t_1, \quad \xi_2 = t_1^v - t_1, \quad \xi_3 = t_2 - t_1^v, \quad \xi_4 = t_2^v - t_2,$$
$$\xi_5 = t_3 - t_2^v, \quad \xi_6 = t_4 - t_3, \quad \xi_7 = t_f - t_4.$$

The arc-parametrization method [16] in combination with the code NUDOCCCS [3] allows to compute the *sensitivity derivatives* $d\xi_i/dp$, $i = 1, \ldots, 7$, with respect to any parameter p in the system. The existence of parametric sensitivity derivatives follows from the fact that second-order sufficient conditions hold for the switching time optimization problem. The precomputation of parametric sensitivity derivatives then enables us to design real-time control approximations to perturbed optimal solutions; cf. the theory and numerical approach in [4, 5]. We consider the following two parameters: the load mass m_2 with nominal value $m_2^0 = 0.56$ and the resistance R with nominal value $R^0 = 2$. In Table 2, we have listed the nominal values ξ_i of the arclengths and the corresponding sensitivity derivatives.

Table 2. Sensitivity derivatives of arclengths: parameters m_2 and R

i	ξ_i	$d\xi_i/dm_2$	$d\xi_i/dR$
1	0.041685	0.008917	0.010355
2	0.0063199	−0.003495	0.001788
3	0.0045841	0.002253	−0.003302
4	0.0037666	0.007321	−0.002233
5	0.022931	0.001764	0.000936
6	0.0092098	0.001446	0.003410
7	0.00075901	0.2879e−6	−0.000449

5.3. Comparison of Numerical Solutions and Experimental Results

The computed optimal control solutions were implemented on the test bench in the IPP mechatronics laboratory, Clausthal University of Technology; cf. Fig. 1. Control signals are applied with the real-time-system sampling time of $T_s = 0.1$ ms ; cf. Table 1. Since the computed minimal times have order of magnitude 0.1 s, approximately 1000 values of the computed optimal control can be used in the experimental test bench. Both for the control bounds $\mathbf{U_{max}} = \mathbf{2}$ and $\mathbf{U_{max}} = \mathbf{3}$, where $v_1(t)$ changes sign, we obtain an excellent agreement between the predicted optimal solution, the simulated solution with 1000 control signals and the experimental solution; cf. Figs. 7, 8.

The small deviations between predicted and measured positions result from friction uncertainties of the guide as well as from noise in the analogue position capturing unit. Positioning times realised at this plant by feedback position control and stepwise reference input are in the

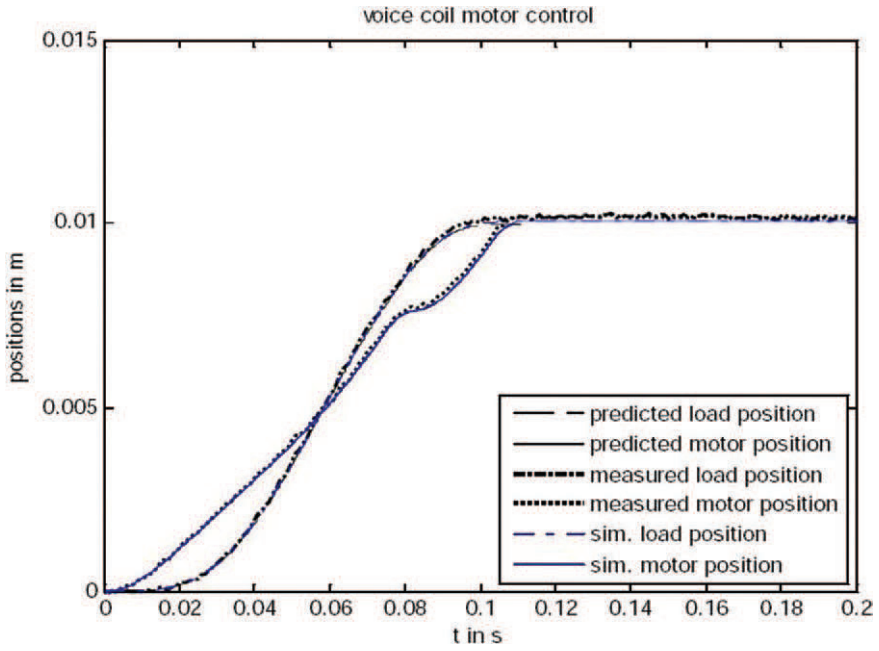

Fig. 7. $\mathbf{U_{max} = 2}$: positions $x_1(t), x_2(t)$; predicted (solid), simulated (dashed), real-time (dashed-dot).

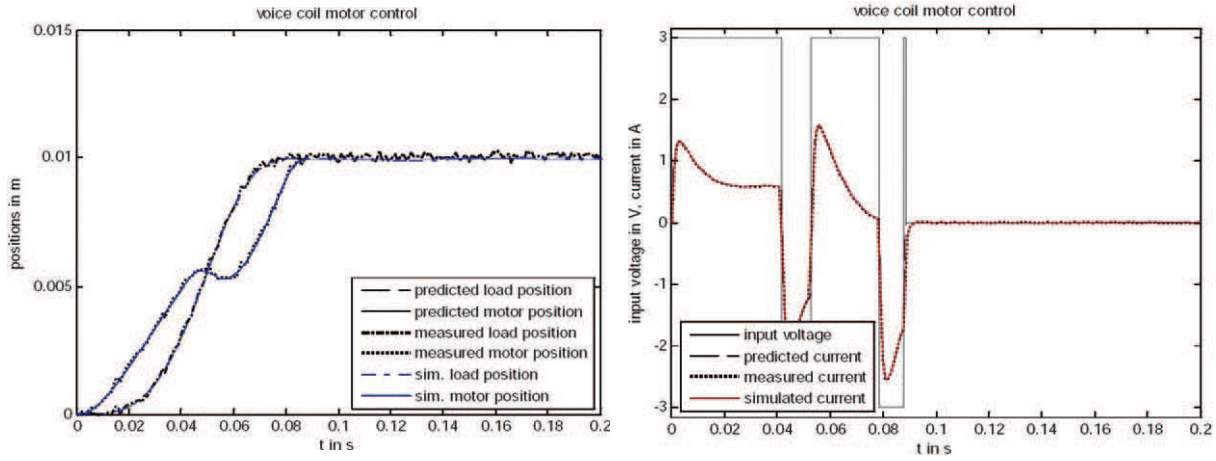

Fig. 8. $\mathbf{U_{max} = 3}$: (a) positions $x_1(t), x_2(t)$, (b) electric current $I(t)$; predicted (solid), simulated (dashed), experimental (dashed-dot).

range of 0.2 s [21] if the step response should be overshoot free. This indicates that the described control method is very efficient.

5.4. State Constraints

Higher values of the voltage control bound $U_{\max}$ lead to higher discrepancies in positions and velocities of the slider and the mass load. Hence, it is reasonable to impose constraints on these deviations. We restrict the discussion to the state constraint $|v_1(t) - v_2(t)| \leq c_v$ for the velocities, which can be written as two inequalities:

$$\begin{aligned} S_1(x) &:= v_1 - v_2 - c_v \leq 0, \\ S_2(x) &:= -c_v - (v_1 - v_2) \leq 0. \end{aligned} \tag{23}$$

Computations show that by using these constraints we can also achieve a significant reduction of the deviation $||x_1 - x_2||_\infty$. We refer the reader to Maurer [15] and Hartl *et al.* [11] for the discussion of necessary conditions for state-constrained optimal control problems. It suffices to analyze the component S_1. The constraint has order 2 since the control variable U appears for the first time in the second time derivative of S_1:

$$\frac{d^2 S_1}{dt^2} = \frac{K_F}{m_1 L}\left(U - RI - K_S v_1\right) - \frac{m_1 + m_2}{m_1 \cdot m_2} K\left(v_1 - v_2\right).$$

A *boundary arc* $[t_{\text{en}}, t_{\text{ex}}]$ for the constraint $S_1(x) \leq 0$ is characterized by the equation $S_1(x(t)) = 0$ for $t_{\text{en}} \leq t \leq t_{\text{ex}}$. Along a boundary arc the equation $d^2 S_1(t)/dt^2 = 0$

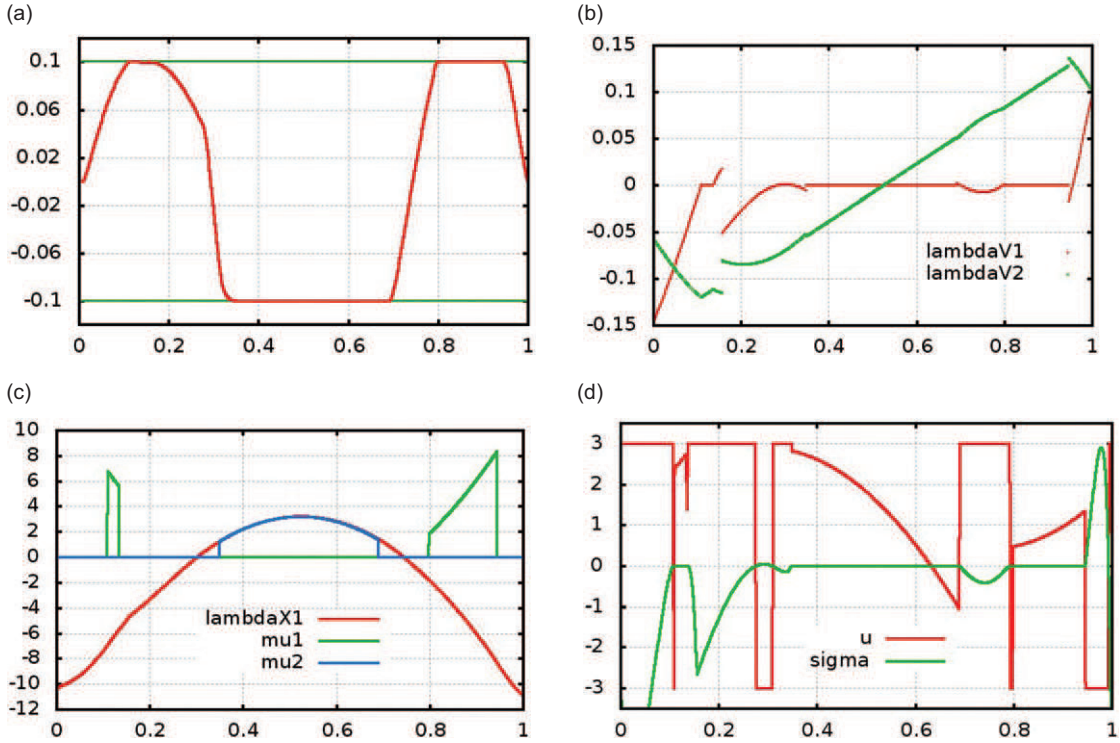

Fig. 9. $\mathbf{U_{max} = 3}$, $|\mathbf{v_1 - v_2}| \leq \mathbf{0.1}$: time–optimal solution on normalized time interval $[0, 1]$ subject to state constraints $|v_1(t) - v_2(t)| \leq 0.1$; (a) difference $v_1(t) - v_2(t)$; (b) adjoints $\lambda_{v_1}(t)$ and $\lambda_{v_2}(t)$ (with jumps); (c) multipliers $\mu_1(t)$, $\mu_2(t)$ and adjoint $\lambda_{x_1}(t)$; (d) control $U(t)$ and scaled switching function $\sigma(t)$.

holds, from which we obtain the following feedback expression for the *boundary control*:

$$U_b(x) = \frac{(m_1 + m_2)KL}{m_2 K_F} \cdot c_v + RI + K_S v_1.$$

The augmented Hamiltonian $\tilde{H}$ is obtained from the Hamiltonian H by adjoining the state constraint with a multiplier $\mu_1 \in \boldsymbol{R}$,

$$\tilde{H}(x, U, \lambda, \mu) = 1 + \lambda(Ax + BU + C\, sign(v_1)) + \mu_1(v_1 - v_2 - c_v).$$

The Minimum Principle [11, 15] implies that the multiplier function satisfies $\mu_1(t) \geq 0$ and $\mu_1(t) = 0$ if $v_1(t) - v_2(t) < c_v$ for all $t \in [0, t_f]$. The adjoint equations (14) are replaced by $\dot{\lambda} = -\tilde{H}_x$, which shows that only the equations for λ_{v_1} and λ_{v_2} are modified:

$$\dot{\lambda}_{v_1} = -\lambda_{x_1} + \lambda_I \frac{K_S}{L} - \mu_1, \quad \dot{\lambda}_{v_2} = -\lambda_{x_2} + \mu_1.$$

It is assumed in [15, 11] that the boundary control $U_b(x(t))$ lies in the interior of the control set. Then it follows from the minimum principle that the switching function vanishes:

$$\frac{1}{L}\lambda_I(t) = \tilde{H}_U(t) = 0 \quad \text{for} \quad t_{\text{en}} \leq t \leq t_{\text{ex}}. \tag{24}$$

This relation allows us to compute the multiplier μ_1. On the boundary arc we have in view of (24),

$$\dot{\lambda}_I = -\lambda_{v_1}\frac{K_F}{m_1} + \lambda_I \frac{R}{L} = -\lambda_{v_1}\frac{K_F}{m_1}, \tag{25}$$

which implies $\lambda_{v_1}(t) = 0$ and thus the relation

$$0 = \dot{\lambda}_{v_1} = -\lambda_{x_1} + \lambda_I \frac{K_S}{L} - \mu_1 = -\lambda_{x_1} - \mu_1. \tag{26}$$

Hence, the multiplier is given by

$$\mu_1(t) = -\lambda_{x_1}(t) \geq 0. \tag{27}$$

In an analogous way, the multiplier for the second state constraint $S_2(x) = -c_v - (v_1 - v_2) \leq 0$ in (23) is computed as $\mu_2(t) = \lambda_{x_2}(t) \geq 0$. These relations are clearly illustrated in Fig. 9(c). Moreover, the adjoint variables λ_{v_1} and λ_{v_2} may have jumps at the entry time and exit time according to

$$\lambda_{v_1}(\tau+) = \lambda_{v_1}(\tau-) - \nu_1(\tau), \quad \nu_1(\tau) \geq 0, \tag{28}$$

$$\lambda_{v_2}(\tau+) = \lambda_{v_2}(\tau-) + \nu_2(\tau), \quad \nu_2(\tau) \geq 0, \tag{29}$$

$\tau \in \{t_{\text{en}}, t_{\text{ex}}\}$, cf. [15, 11].

Fig. 9 displays the optimal solution for the rather restrictive bound $c_v = 0.1$. The structure of the optimal control is complicated, since there are two boundary arcs with $v_1(t) - v_2(t) = c_v$, one boundary arc with

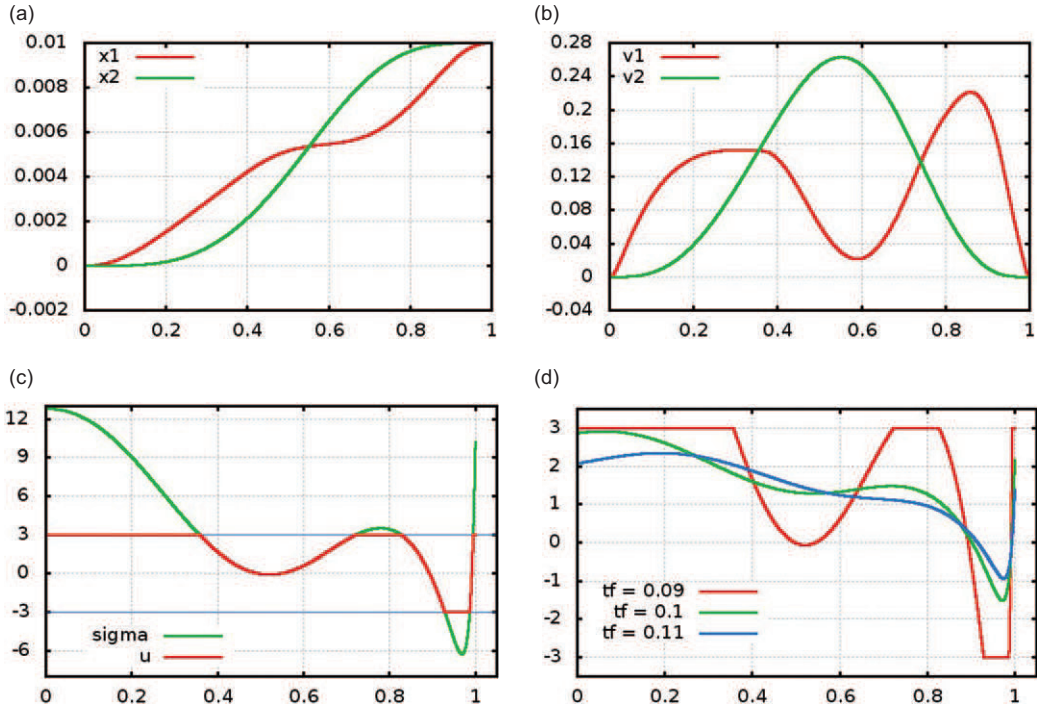

Fig. 10. $\mathbf{U_{max} = 3}$: energy-optimal solutions on normalized time interval $[0, 1]$; (a) positions $x_1(t), x_2(t)$ for final time $t_f = 0.09$, (b) velocities $v_1(t), v_2(t)$ for final time $t_f = 0.09$, (c) optimal control $U(t)$ and $\sigma(t) = -\lambda_I/2L$ for final time $t_f = 0.09$ (d) optimal control for final times $t_f = 0.09$, $t_f = 0.1$, $t_f = 0.11$.

$v_1(t) - v_2(t) = -c_v$ and 10 interior bang-bang arcs. The final time $t_f = 0.098725$ is about 11.5% higher than in the unconstrained case; cf. 5.1.

6. Energy-Optimal Control

In this section, we consider the "energy-optimal" cost functional (11) of minimizing

$$\int_0^{t_f} U(t)^2 dt \tag{30}$$

with a fixed final time $t_f > t_{min}$, where t_{min} is the minimal time computed in section 5.1. In this case, the Hamiltonian

$$H(x(t), \lambda(t), U) = U^2 + \lambda(t)(Ax(t) + B \cdot U + C \operatorname{sign}(v_1(t)))$$

is regular and admits a unique minimizer

$$U(t) = Proj_{[-U_{\max}, U_{\max}]}(-\lambda_I(t)/2L),$$

where *Proj* denotes the projection onto the control set. Fig. 10(c) confirms this control law. The adjoints satisfy the same adjoint equations as in the time-optimal case, cf. (14). In particular, it follows that the Hamiltonian is regular and any optimal control $U(t)$ is *continuous*. It is well known that the quadratic cost functional smoothes the structure of the optimal control. Using the control bound

Table 3. Differences in positions and velocities for time-optimal ($t_f = 0.088618$) and energy-optimal solutions ($t_f = 0.09, 0.1, 0.11$)

t_f	$\|x_1 - x_2\|_\infty$	$\|v_1 - v_2\|_\infty$
0.088618	0.002979	0.337792
0.09	0.002174	0.238127
0.1	0.001940	0.150524
0.11	0.001594	0.111915

$U_{\max} = 3$, Fig. 10(d) depicts optimal solutions for 3 final times that differ from the minimal time $t_{\min} = 0.088618$ by less than 25%. Note that already for the final time $t_f = 0.09$ the velocity $v_1(t)$ does not change sign. In this case, the optimal solution consists of four boundary arcs and three interior arcs.

A practical side-effect of energy-optimal controls is that they reduce oscillations in positions and velocities with increasing final time; cf. Table 3. As an example, consider the energy-optimal functional, where the final time t_f is increased by only 1.5%, $t_f = 1.015 \cdot t_{\min}$. It is remarkable that the maximum difference $||v_1 - v_2||_\infty$ in the velocities is reduced by 30 % compared to the time-optimal case.

7. Conclusion

An optimal control problem for an electrodynamical servo drive system, the voice-coil motor, was formulated. The

Coulombic friction force gives rise to state-dependent jumps in the dynamical system. This feature leads us to consider a nonsmooth control problem, when the velocity of the slider changes sign. We showed that time-optimal controls are bang-bang and determined those control bounds for which the slider velocity changed sign. The arc-parametrization method in [16] in conjunction with the routine NUDOCCCS [3, 5] were applied to directly optimizing the switching times. We could observe an excellent agreement between the computed optimal trajectories and experimental results on a test bench developed by the third author. Oscillations in the positions and velocities can be significantly reduced by either imposing state inequality constraints or determining energy-optimal solutions which, however, need larger process durations.

One last but very interesting result of our study is the fact, that time or energy-optimal control of the input variable allows much better positioning results than state-of-the-art feedback control. We expect that further investigations for different servo axis applications can yield hints for the setpoint generation in the numerical control system in order to reach the time optimal control performance also with feedback control structures.

We became aware of the recent work of Kim *et al.* [13], in which a similar but simpler time-optimal control model was discussed. The authors use a different numerical approach which, however, does not provide adjoint variables to test necessary conditions. It would be of interest to apply the methods of this paper to the model in [13].

Acknowledgements

B. Christiansen and H. Maurer gratefully acknowledge the support of the Deutsche Forschungsgemeinschaft under grant MA/691-2. Authors are grateful to anonymous reviewers for helpful comments.

References

1. Agrachev AA, Stefani G, Zezza PL. Strong optimality for a bang–bang trajectory. *SIAM J Control Optim* 2002; 41: 991–1014.
2. Augustin D, Maurer H. Second order sufficient conditions and sensitivity analysis for optimal multiprocess control problems. *Control Cybern* 2000; 29: 11–31.
3. Büskens C. *Optimierungsmethoden und Sensitivitätsanalyse für optimale Steuerprozesse mit Steuer- und Zustands-Beschränkungen*. Dissertation, Institut für Numerische Mathematik, Universität Münster, 1998.
4. Büskens C, Maurer H. Sensitivity analysis and real-time optimization of parametric nonlinear programming problems. In: Grötschel, Krumke S, Rambaum D (eds), in *Online Optimization of Large Scale Systems.* Springer–Verlag, Berlin 2001; 3–16.
5. Büskens C, Maurer H. SQP–methods for solving optimal control problems with control and state constraints: adjoint variables, sensitivity analysis and real–time control. *J Comput Appl Math* 2000; 120: 85–108.
6. Christiansen B, Maurer H, Zirn O. *Time-optimal control of a voice-coil motor with Coulombic friction.* In Proceedings of the 47th IEEE Conference on Decision and Design, Cancun, Mexico, December 9–11, 2008; 1557–1562.
7. Clarke FH, Vinter RB. Optimal multiprocesses. *SIAM J Control Optim* 1989; 27: 1072–1091.
8. Clarke FH, Vinter RB. Applications of optimal multiprocesses. *SIAM J Control Optim* 1989; 27: 1048–1071.
9. Fourer R, Gay DM, Kernighan BW. *AMPL: A Modeling Language for Mathematical Programming*. Duxbury Press, Brooks–Cole Publishing, 1993.
10. Fourer R, Gay DM, Kernighan BW. *The AMPL Book*. Duxbury Press, Brooks–Cole Publishing, 2002.
11. Hartl RF, Sethi SP, Vickson RG. A survey of the maximum principles for optimal control problems with state constraints. *SIAM Rev* 1995; 17: 181–218.
12. Hermes H, LaSalle JP. *Functional Analysis and Time Optimal Control*. Academic Press, New York, 1969.
13. Kim JJ, Kased R, Singh T. Time-optimal control of flexible systems subject to friction. *Optim Control Appl Methods* 2008; 29: 257–277.
14. Kim JHR, Maurer H. *Sensitivity analysis of optimal control problems with bang-bang controls.* In Proceedings of the 42nd IEEE Conference on Decision and Control, Maui, USA, IEEE Society, 2003; 3281–3286.
15. Maurer H. *On the minimum principle for optimal control problems with state constraints*, Schriftenreihe des Rechenzentrums der Universität Münster, ISSN 0344-0842, 1977.
16. Maurer H, Büskens C, Kim JHR, Kaya CY. Optimization methods for the verification of second order sufficient conditions for bang–bang controls. *Optim Control Appl Methods* 2005; 26: 129–156.
17. Maurer H, Osmolovskii NP. Second order sufficient conditions for time–optimal bang–bang control problems. *SIAM J Control Optim* 2004; 42: 2239–2263.
18. Milyutin AA, Osmolovskii NP. *Calculus of Variations and Optimal Control, Translations of Mathematical Monographs*, vol 180. American Mathematical Society, 1998.
19. Osmolovskii NP, Maurer H. Equivalence of second order optimality conditions for bang-bang control problems. Part 1: Main results, *Control Cybern* 2005; 34: 927–950; Part 2: Proofs, variational derivatives and representations, *Control Cybern* 2007; 36: 5–45.
20. Wächter A, Biegler LT. On the implementation of a primal-dual interior point filter line search algorithm for large-scale nonlinear programming. *Math Program* 2006; 106: 25–57 (cf. also http://www.coinor.org/Ipopt/documentation/).
21. Zirn O. Machine Tool Analysis: *Modelling, simulation and control of machine tool manipulators*, Habilitation thesis, Department of Mechanical and Process Engineering, Swiss Federal Institute of Technology (ETH) Zürich, 2008.